Measuring Black Hole Spin by the Continuum-Fitting Method: Effect of Deviations from the Novikov-Thorne Disc Model

Monthly Notices
of the
ROYAL ASTRONOMICAL SOCIETY

Mon. Not. R. Astron. Soc. **414,** 1183–1194 (2011) doi:10.1111/j.1365-2966.2011.18446.x

Measuring black hole spin by the continuum-fitting method: effect of deviations from the Novikov–Thorne disc model

Akshay K. Kulkarni,[1⋆] Robert F. Penna,[1⋆] Roman V. Shcherbakov,[1⋆] James F. Steiner,[1⋆] Ramesh Narayan,[1⋆] Aleksander Sądowski,[2⋆] Yucong Zhu,[1⋆] Jeffrey E. McClintock,[1⋆] Shane W. Davis[3⋆] and Jonathan C. McKinney[4⋆]

[1]*Harvard-Smithsonian Center for Astrophysics, 60 Garden St, Cambridge, MA 02138, USA*
[2]*Nicolaus Copernicus Astronomical Center, Bartycka 18, PL 00-716, Warsaw, Poland*
[3]*Canadian Institute for Theoretical Astrophysics, Toronto, ON M5S3H4, Canada*
[4]*Department of Physics and Kavli Institute for Particle Astrophysics and Cosmology, Stanford University, Stanford, CA 94305-4060, USA*

Accepted 2011 January 31. Received 2011 January 29; in original form 2010 October 28

ABSTRACT

The X-ray spectra of accretion discs of eight stellar mass black holes have been analysed to date using the thermal continuum-fitting method, and the spectral fits have been used to estimate the spin parameters of the black holes. However, the underlying model used in this method of estimating spin is the general relativistic thin-disc model of Novikov & Thorne, which is only valid for razor-thin discs. We therefore expect errors in the measured values of spin due to inadequacies in the theoretical model. We investigate this issue by computing spectra of numerically calculated models of thin accretion discs around black holes, obtained via three-dimensional general relativistic magnetohydrodynamic (GRMHD) simulations. We apply the continuum-fitting method to these computed spectra to estimate the black hole spins and check how closely the values match the actual spin used in the GRMHD simulations. We find that the error in the dimensionless spin parameter is up to about 0.2 for a non-spinning black hole, depending on the inclination. For black holes with spins of 0.7, 0.9 and 0.98, the errors are up to about 0.1, 0.03 and 0.01, respectively. These errors are comparable to or smaller than those arising from current levels of observational uncertainty. Furthermore, we estimate that the GRMHD simulated discs from which these error estimates are obtained correspond to effective disc luminosities of about 0.4–0.7 Eddington, and that the errors will be smaller for discs with luminosities of 0.3 Eddington or less, which are used in the continuum-fitting method. We thus conclude that use of the Novikov–Thorne thin-disc model does not presently limit the accuracy of the continuum-fitting method of measuring black hole spin.

Key words: accretion, accretion discs – black hole physics – MHD – methods: numerical – X-rays: binaries.

1 INTRODUCTION

Astrophysical black holes are described by just two parameters: their mass M and angular momentum J, with the latter usually expressed in terms of the dimensionless spin parameter $a_* = cJ/GM^2$. While the mass M is relatively straightforward to obtain using dynamical measurements, the spin parameter a_* is less so. In accreting black holes, however, emission from the inner disc gives us a handle on the spin. According to the model developed by Novikov & Thorne (1973, hereafter NT)[1] for a razor-thin accretion disc around a black hole, viscous evolution causes the accreting matter to move slowly inwards along nearly Keplerian orbits until reaching the radius of the innermost stable circular orbit (ISCO), after which the gas plunges into the black hole on a dynamical time-scale. Thus, the inner edge of the viscous accretion disc is predicted to be very close to the ISCO. This link between the radius of the ISCO, $r_{\rm ISCO}$, and

⋆E-mail: akulkarni@cfa.harvard.edu (AKK); rpenna@cfa.harvard.edu (RFP); rshcherbakov@cfa.harvard.edu (RVS); jsteiner@cfa.harvard.edu (JFS); rnarayan@cfa.harvard.edu (RN); as@camk.edu.pl (AS); yzhu@cfa.harvard.edu (YZ); jem@head.cfa.harvard.edu (JEM); swd@cita.utoronto.ca (SWD); jmckinne@stanford.edu (JCM)

[1] This is the relativistic generalization of the standard thin-disc model of Shakura & Sunyaev (1973).

the radius of the inner edge of the disc, $r_{\rm in}$, is well supported by empirical evidence that the inner radius is constant in disc-dominated states of black hole binaries (Narayan, McClintock & Shafee 2008; Steiner et al. 2010a, and references therein), and by recent general relativistic magnetohydrodynamic (GRMHD) simulations of thin accretion discs (Shafee et al. 2008a; Penna et al. 2010; but see Noble, Krolik & Hawley 2009, 2010). Therefore, measuring $r_{\rm in}$ gives one an estimate of $r_{\rm ISCO}$. Since $r_{\rm ISCO}/M$ is a monotonic function of a_* (e.g. Shapiro & Teukolsky 1983), we can then obtain the spin of the black hole. This is the main technique currently being used to estimate the spins of stellar mass black holes in binary systems.

One of the ways of measuring $r_{\rm in}$ involves[2] fitting the thermal X-ray continuum spectrum from the disc with the NT model spectrum (e.g. Zhang, Cui & Chen 1997; Shafee et al. 2006; Davis, Done & Blaes 2006; Gou et al. 2009, 2010; Steiner et al. 2009, 2010a) using models such as KERRBB (Li et al. 2005) and BHSPEC (Davis & Hubeny 2006) in the data-analysis package XSPEC (Arnaud 1996). From the fit, one obtains $r_{\rm in}$, or equivalently, a_*, if suitable estimates of the black hole mass, inclination and distance are available (e.g. see Gou et al. 2009). Both KERRBB and BHSPEC assume that the structure of the disc and its emission properties are described accurately by the NT model.

It is therefore clear that a crucial issue in black hole spin estimation via the continuum-fitting method is the NT model and its reliability. How much do real accretion discs with finite thickness differ from the NT disc? This question was addressed by Paczyński (2000) and Afshordi & Paczyński (2003), who argued that deviations from the NT model decrease monotonically with decreasing disc thickness and that thin discs with dimensionless thickness $|h/r| \ll 1$ are well described by the model, if the viscosity parameter $\alpha \ll 1$. Their argument was confirmed by detailed calculations carried out by Shafee, Narayan & McClintock (2008b). This still leaves open the question of whether *magnetized* discs might deviate substantially from the NT model even at small disc thicknesses (Krolik 1999). A number of recent studies of magnetized discs using 3D GRMHD simulations, including Shafee et al. (2008a), Noble et al. (2009, 2010) and Penna et al. (2010), have explored this question. These authors estimate that the luminosity and stress of the inner regions of simulated discs differ from the NT model by factors ranging from a few per cent (Penna et al. 2010) to as much as 20 per cent (Noble et al. 2009). The question then is how much this departure affects measurements of black hole spin.

We investigate this question using a very straightforward approach: we start with a disc model obtained via the above-mentioned GRMHD simulations (principally models similar to those described in Penna et al. 2010), compute the disc emission as a function of radius using a local blackbody approximation (assuming a constant spectral hardening factor), and use ray-tracing to compute the spectra. We then fit these spectra using KERRBB and compare the resulting spin estimate with the spin that was used in the GRMHD simulation. Our goal is similar to that of Shafee et al. (2008b), who performed the same analysis for a purely hydrodynamical disc, and of Li, Yuan & Cao (2010); the important difference between the latter work and ours is that we use disc models obtained from GRMHD simulations, although we do not explore the effect of a finite photospheric height in detail. Analogous work (though with a pseudo-Newtonian, not GRMHD, code) on the systematic errors in spin estimates obtained by fitting the broad iron emission lines from the inner accretion disc has been done by Reynolds & Fabian (2008).

We begin in Section 2 with a description of our method, and calculate in Section 3 the error in black hole spin estimates due to deviations of GRMHD discs from the NT model. We discuss in Section 4 the observational uncertainties in black hole spin determination and compare these with the errors arising from use of the NT model. We conclude in Section 5 with a summary. Some technical details are discussed in Appendices A, B and C.

2 METHOD

2.1 Calculation of disc temperature and velocity profiles from GRMHD simulations

We work in Boyer–Lindquist (BL) coordinates $x^\alpha = (t, r, \theta, \phi)$. We use geometric units where the speed of light c, the gravitational constant G and the Planck's constant are set to unity, and measure all lengths and times in units of the black hole mass M.

For this project, we reran the 3D GRMHD simulations of thin discs described in Penna et al. (2010), for four values of the black hole spin: $a_* = 0, 0.7, 0.9, 0.98$. For completeness, we briefly review the simulation setup here. The simulations solve the GRMHD equations for plasma around a rotating black hole using the code HARM (Gammie, McKinney & Tóth 2003) with numerous recent improvements, including 3D capabilities (McKinney 2006; McKinney & Blandford 2009). The gas is initially in a torus in hydrodynamic equilibrium surrounding the black hole (De Villiers, Hawley & Krolik 2003; Gammie et al. 2003). The spin axes of the torus and the black hole are aligned. The torus is seeded with a magnetic field consisting of four poloidal loops arranged in the radial direction. We use a polytropic equation of state for the gas, $p \propto \rho^\gamma$, where p, ρ and γ are the pressure, density and adiabatic index respectively, and choose $\gamma = 4/3$ as appropriate for a radiation pressure dominated disc.

To keep the disc thin, we use a simple cooling prescription that drives the gas to its initial entropy on a dynamical time-scale.[3] The energy removed by the cooling prescription is assumed to be completely lost by the accretion flow; it has no dynamical effect on the accreting gas (the energy lost to cooling is of course tracked and is later used to compute the disc luminosity profiles shown in Fig. 1). The disc thickness is specified by the quantity $|h/r|$, where h is the density scaleheight of the disc above the mid-plane, $|h| = \int \rho\,|z|\,{\rm d}z / \int \rho\,{\rm d}z$, and r is the cylindrical radius. Our simulated thin discs have $|h/r| = 0.05, 0.04, 0.05$ and 0.08 respectively for $a_* = 0, 0.7, 0.9$ and 0.98. Following Penna et al. (2010), we perform a temporal and azimuthal average over the steady-state portion of the simulation results to average over the fluctuations introduced by turbulence, since we are interested in the mean behaviour of the accretion flow. Finally, since our discs are geometrically thin, we perform a density-weighted average in the polar direction to obtain the vertically integrated disc structure. This process of collapsing the simulated disc into the equatorial plane circumvents the difficulty of defining a photosphere for the disc and calculating emission profiles along it. A proper treatment would require a full radiative transfer

[2] Another method involves fitting the profile of the relativistically broadened iron line (e.g. Fabian et al. 1989, 2000; Laor 1991; Reynolds & Nowak 2003; Brenneman & Reynolds 2006).

[3] One change from Penna et al. (2010) is that in the present work we cool all the gas, including the gas in the corona, whereas in most of their simulations, Penna et al. cooled only the disc region of the flow. The present simulations are similar to the 'no-tapering model' described in Section 5.7 and fig. 13 of their paper.

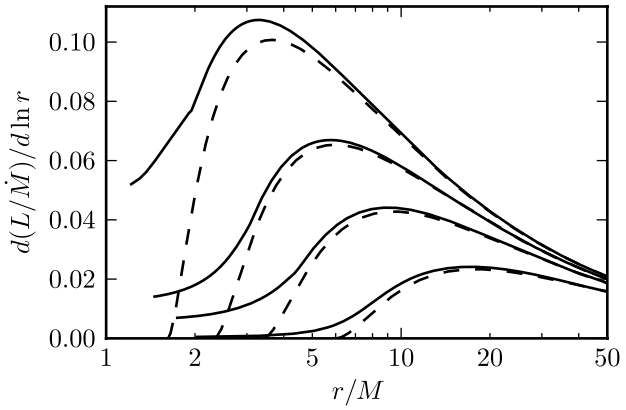

Figure 1. Luminosity profiles from the GRMHD simulations (solid lines) compared with those from the NT model (dashed lines) for $a_* = 0$, 0.7, 0.9 and 0.98 (bottom to top). The disc thicknesses are $|h/r| = 0.05$, 0.04, 0.05 and 0.08 respectively for these runs. The ISCO is located at the radius where the NT disc luminosity goes to zero.

calculation (e.g. Davis et al. 2005; Sądowski et al. 2011), which is beyond the scope of this work.

At the end of this process, both components required to calculate the spectra are available: the radial profile of the fluid four-velocity $u^\mu(r)$ in the equatorial plane and, from the energy removed by the cooling prescription,[4] the profile of the emitted flux $F(r) \equiv \mathrm{d}E/(r\mathrm{d}r\mathrm{d}\phi\mathrm{d}t)$ (where E is the energy emitted from one side of the disc as measured by an observer at infinity). When calculating the spectrum, the effect of electron scattering in the disc is taken into account indirectly using a colour correction (or spectral hardening) factor $f_{\rm col}$. For the results presented here, we choose for simplicity a fiducial value of $f_{\rm col} = 1.7$ (Shimura & Takahara 1995). Detailed models of disc atmospheres by Davis et al. (2005) and Davis & Hubeny (2006) indicate that $f_{\rm col}$ can vary between 1.4 and 1.7, but this extra sophistication is not necessary for the simple tests described in the present paper.

The flux profiles obtained from the GRMHD simulations are only reliable within a radius inside which the accretion flow has reached steady state. Outside this radius, which we call the inflow equilibrium radius $r_{\rm ie}$ (see Penna et al. 2010, for a definition), we extend the profiles using the analytical disc model of Page & Thorne (1974). The procedure we use is described in Appendix A. Within a certain range, the exact choice of $r_{\rm ie}$ does not affect the results of the extrapolation, as we show in that appendix.

Fig. 1 compares the luminosity profiles $\mathrm{d}(L/\dot{M})/\mathrm{d}(\ln r)$ that we obtain to those in the standard NT disc model, for four values of the spin: $a_* = 0$, 0.7, 0.9, 0.98. Here, $\dot{M}$ is the accretion rate, and the luminosity $L \equiv 2\mathrm{d}E/\mathrm{d}t = 2\int Fr\mathrm{d}r\mathrm{d}\phi = 4\pi\int Fr\mathrm{d}r$, so $\mathrm{d}(L/\dot{M})/\mathrm{d}(\ln r) = 4\pi r^2 F(r)/\dot{M}$ (the extra factor of 2 is to account for emission from both sides of the disc).

The NT model has no radiation from inside the ISCO, whereas the simulations show some emission from this region. In addition, the peak of the emission in the simulated discs is seen to shift inwards relative to the NT model. These effects are similar to those obtained by Sądowski (2009) for slim discs. As explained in that work, for large enough accretion rates ($\gtrsim$0.3 Eddington), the accretion flow starts becoming radiatively inefficient at moderate radii ($r \sim 10$–$30M$); as a result, some of the heat generated by viscous dissipation at larger radii is advected inwards and released at smaller radii. Another important effect is that discs with finite thickness have a non-vanishing stress at the ISCO (in contrast to the razor-thin discs which the NT model considers for which the stress is expected to vanish). This stress leads to additional viscous dissipation at radii $r \sim r_{\rm ISCO}$. In our model, the inward shift in the emission peak due to both of these effects mimics a decrease in $r_{\rm ISCO}$ (see Fig. 1), i.e. an increase in the predicted black hole spin. As a result, fitting the GRMHD disc spectrum using the NT model leads to an overestimate of the black hole spin, as we shall see in Section 3.

[4] We only include the energy removed from the bound gas, since including all the gas results in an overestimate of the luminosity (Penna et al. 2010).

2.2 Calculation of the spectra

To calculate the spectrum, we assume that the flux $F(r)$ is emitted in the form of colour-corrected blackbody radiation ($f_{\rm col} = 1.7$), either isotropically or with limb-darkening, as seen in the comoving frame of the fluid. We use a standard limb-darkening prescription (equation 5 below). We assume that after emission the radiation propagates in vacuum.

Were the accretion disc non-relativistic, the calculation of the spectrum would be almost trivial (see e.g. Frank, King & Raine 2002): one would divide the disc into annuli; define an effective blackbody temperature $T_{\rm eff}(r) = [F(r)/\sigma]^{1/4}$ in each annulus, where σ is the Stefan–Boltzmann constant; use the temperature and colour-correction factor to obtain the specific intensity $I_{\nu,\rm disc}(r)$ of the emitted radiation at the disc surface and integrate it over the disc surface to obtain the observed spectrum.

Relativity introduces three complications: (1) The effective temperature has to be defined in the comoving frame of the fluid, and so we need to transform $F(r)$ from the BL frame into the comoving frame. (2) Redshift between the comoving frame and the observer's frame, both gravitational and due to Doppler boosting, has to be taken into account. Since the photon paths around a black hole are complicated, the direction in which a ray needs to be emitted in the comoving frame such that it reaches the observer is not known a priori, which is a problem for the redshift calculation. (3) One needs to know the emission direction to take limb darkening into account as well. Points (2) and (3) require integrating the geodesic equations to calculate the photon paths, which is usually referred to as 'ray-tracing'. This approach has been applied extensively in the literature to a variety of problems, starting with Cunningham & Bardeen (1973) and Cunningham (1975) (see Dexter & Agol 2009 and references therein). In particular, KERRBB (Li et al. 2005) uses this technique to compute thin-disc spectra.

We perform ray-tracing numerically using the routines developed by Shcherbakov & Huang (2011) and applied in Shcherbakov, Penna & McKinney (2010). We choose a line of sight to the observer with an inclination angle of i relative to the black hole spin axis. At a sufficiently large distance from the black hole ($r \sim 10^5$), we set up an image plane perpendicular to the line of sight and shoot rays from it parallel to the line of sight. We follow these rays until they hit the disc,[5] by directly integrating the (second-order) geodesic equations:

$$\frac{\mathrm{d}^2x^\alpha}{\mathrm{d}\lambda^2} + \Gamma^\alpha_{\beta\gamma}\frac{\mathrm{d}x^\beta}{\mathrm{d}\lambda}\frac{\mathrm{d}x^\gamma}{\mathrm{d}\lambda} = 0, \quad (1)$$

[5] This is more straightforward than shooting rays from the disc, since as mentioned earlier, the direction in which the rays need to be emitted from the disc such that they reach the observer is not known a priori. This approach was pioneered by Marck (1996); see also Hameury, Marck & Pelat (1994).

where λ is an affine parameter along the geodesic, and $\Gamma^{\alpha}_{\beta\gamma}$ are the connection coefficients. The aim is to obtain the specific intensity I_ν of each ray, which can then be integrated over the image plane to obtain the observed flux:

$$F_{\nu,\rm obs} = \frac{1}{D^2}\int I_\nu {\rm d}A. \tag{2}$$

Since I_ν/ν^3 is a Lorentz invariant, we can immediately relate the specific intensity I_ν in the image plane to the intensity $I_{\nu,\rm com}$ in the comoving frame of the fluid at the point of emission:

$$I_\nu = I_{\nu,\rm com}\,(\nu/\nu_{\rm com})^3 \equiv I_{\nu,\rm com}\chi^3, \tag{3}$$

where $\chi \equiv \nu/\nu_{\rm com}$ is the redshift factor, and

$$I_{\nu,\rm com} = \frac{2f_{\rm col}^{-4}\nu_{\rm com}^3}{\exp(\nu_{\rm com}/k_{\rm B}f_{\rm col}T_{\rm com})-1}\Upsilon. \tag{4}$$

Here, $f_{\rm col}$ is the spectral hardening factor mentioned earlier, which we set to 1.7 in this work, and Υ is the limb-darkening factor (see e.g. Li et al. 2005):

$$\Upsilon = \begin{cases} 1, & \text{isotropic emission} \\ \frac{1}{2}+\frac{3}{4}\cos\theta_{\rm com}, & \text{limb-darkened emission.} \end{cases} \tag{5}$$

So finally we have

$$I_\nu = \frac{2f_{\rm col}^{-4}\nu^3}{\exp(\nu/k_{\rm B}f_{\rm col}\chi T_{\rm com})-1}\Upsilon, \tag{6}$$

or

$$F_{\nu,\rm obs} = \frac{1}{D^2}\int \frac{2f_{\rm col}^{-4}\nu^3}{\exp(\nu/k_{\rm B}f_{\rm col}\chi T_{\rm com})-1}\Upsilon {\rm d}A. \tag{7}$$

Thus, to calculate the spectrum, we need the effective temperature in the comoving frame $T_{\rm com}$, the redshift factor χ and the angle $\theta_{\rm com}$ between the emitted ray and the disc normal in the comoving frame. The first of these is obtained by transforming the emitted flux $F(r)$, which is initially calculated in the BL frame, into the comoving frame, and the last two by transforming the ray four-momentum. We show the details in Appendix B.

To calculate spectra using equation (7), we use the following fiducial parameters: black hole mass $M = 10\,{\rm M}_\odot$, accretion rate $\dot{M} = 0.1\dot{M}_{\rm Edd}$ and distance to the black hole $D = 10\,{\rm kpc}$. We choose a spectral energy range of 0.1–10 keV, divided into 1000 logarithmically spaced bins. Fig. 2 compares the spectra from the simulated and NT discs for $a_* = 0.9$ and $i = 75^\circ$. The peak of the spectrum of the simulated disc is shifted to a slightly higher energy relative to the NT spectrum, and the peak flux is also higher. This is precisely the effect that increasing the black hole spin would have on the NT spectrum, and as we shall see in Section 3, fitting the simulated spectra leads one to overestimate the spin.

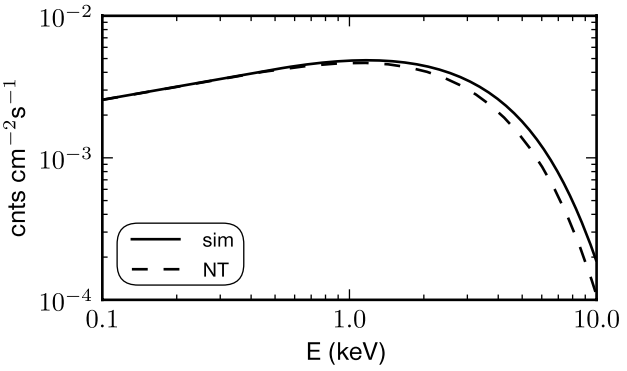

Figure 2. Spectra from the simulated (solid line) and NT (dashed line) discs, for $a_* = 0.9$ and $i = 75^\circ$.

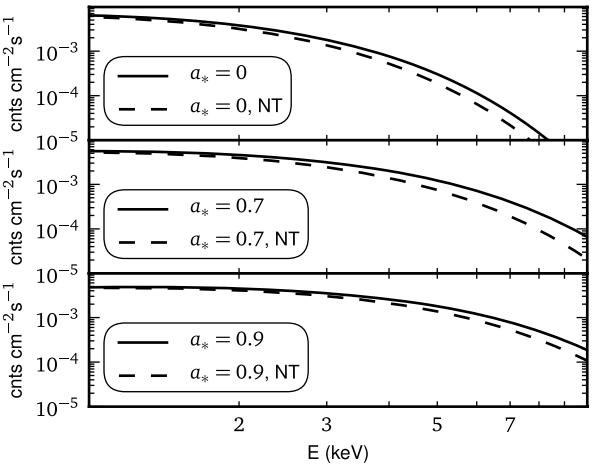

Figure 3. High-energy portion of the spectra from the simulated (solid lines) and NT (dashed lines) discs, for $i = 75^\circ$ and three values of the black hole spin: $a_* = 0, 0.7, 0.9$.

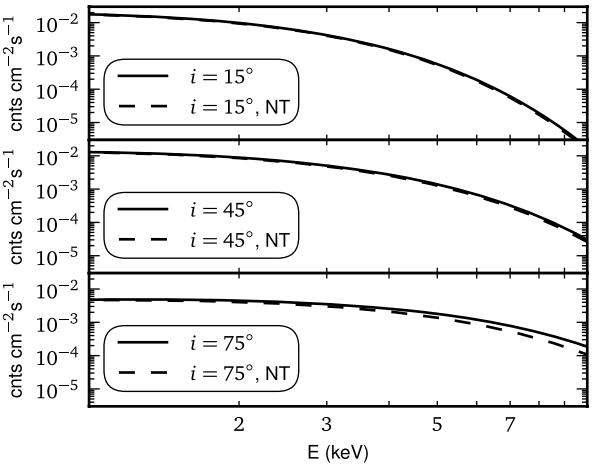

Figure 4. High-energy portion of the spectra from the simulated (solid lines) and NT (dashed lines) discs, for $a_* = 0.9$ and three inclinations: $i = 15^\circ, 45^\circ, 75^\circ$.

Figs 3 and 4 show what happens to the difference between the simulated and NT spectra when we vary the spin and the inclination, respectively. The effect is visible at the high-energy end of the spectrum. The effect of the inclination is very strong. This is because of the excess luminosity from the inner region of the simulated disc; this excess is more noticeable at higher inclinations due to beaming of the emitted radiation.

2.3 Tests

We tested our code by comparing the spectra it produces for an NT disc to those produced by KERRBB itself using the 'fakeit' command in XSPEC, for the following range of parameters: black hole masses of 5, 10, 15 $\rm M_\odot$; spin parameters $a_* = 0, 0.7, 0.9$; observer inclinations

$i = 15^\circ, 45^\circ, 75^\circ$; accretion rates $\dot{M}/\dot{M}_{\rm Edd} = 0.1,\ 0.2$ and distances $D = 10,\ 20$ kpc, with and without using limb darkening. At a grid resolution of $N_b \times N_\beta = 100 \times 100$ (see the description of our grid in Appendix C), the spectra calculated with our code converge to the KERRBB spectra in all these cases. This confirms that the code is robust.

3 RESULTS

We use the following fiducial parameters for our spectra, as mentioned earlier: black hole mass $M = 10\,{\rm M}_\odot$, accretion rate $\dot{M} = 0.1\dot{M}_{\rm Edd}$ and distance to the black hole $D = 10$ kpc. The spectra are fitted using KERRBB (without using returning radiation, since we do not include it in our spectrum calculation) to obtain the black hole spin a_* and accretion rate $\dot{M}$.

One more thing needs to be taken care of. Even though we average the GRMHD simulation results azimuthally and over time to remove the effects of turbulence and obtain a mean profile for the flux $F(r)$ and the gas four-velocity $u^\mu(r)$, there is still some stochastic variation in the spin estimates with time. Therefore, we divide the steady-state portion of each simulation into chunks of duration $\Delta t = 1000M$ (each simulation has 4–5 such chunks), obtain a spin estimate from each chunk, and then quote the mean spin estimate and the error in the mean for each simulation.[6]

The results for limb-darkened emission[7] are shown in columns 1, 3, 4 and 5 of Table 1. As expected, the fitted values are different than the ones used in the GRMHD simulations. The differences are largest at low spins. It is easy to understand why the difference is not constant; the dependence of the disc temperature profile (which determines the shape of the spectrum) on the spin is highly nonlinear. In particular, the position of the spectral peak in the NT model strongly depends on the radius of the ISCO ($r_{\rm ISCO}$), to the extent that one can think of KERRBB as fitting for $r_{\rm ISCO}$ instead of a_*. There is a one-to-one relationship between a_* and $r_{\rm ISCO}$ (see, e.g. Shapiro & Teukolsky 1983), shown in Fig. 5. At high spins, $r_{\rm ISCO}$ varies very rapidly as a function of a_*; conversely, a_* varies relatively slowly as a function of $r_{\rm ISCO}$. Thus, a given fractional error in $r_{\rm ISCO}$ translates into a much smaller error in a_* at higher spins than at smaller ones. This is illustrated by the two grey bands in Fig. 5. Each band represents a range of ± 10 per cent in $r_{\rm ISCO}$, around $r_{\rm ISCO} = 6$ (upper band, corresponding to $a_* = 0$) and $r_{\rm ISCO} = 1.61$ (lower band, corresponding to $a_* = 0.98$). The corresponding range in a_* is ± 0.2 at $a_* = 0$, but only ± 0.01 at $a_* = 0.98$.

For reference, we show the errors in the estimated $r_{\rm ISCO}$ in Table 2 (the exact values of $r_{\rm ISCO}$ for $a_* = 0, 0.7, 0.9$ and 0.98 are $6, 3.39, 2.32$ and 1.61), and the fitted accretion rates in Table 3 [the fiducial rate of $0.1\dot{M}_{\rm Edd}$ used here corresponds to $(2.45, 1.35, 0.898, 0.5982) \times 10^{18}\,{\rm g\,s^{-1}}$ for the four spins, assuming that the accretion efficiencies are given by their NT values]. It is interesting to note that although the errors in the fitted spins are relatively large, the errors in the accretion rates are only a few per cent.

The other important effect is that of the observer inclination: at high inclination, the error in the spin estimate is larger. This is because the difference between the disc temperature profiles in the NT model and the simulations is significant only in the inner disc. At low inclination angles, the combined effect of gravitational redshift and beaming of the radiation (the latter of which concentrates the radiation close to the equatorial plane) results in this difference not being noticeable in the spectrum. At high inclination angles, on the contrary, beaming enhances the difference, causing the error in the fitted spin to increase.

Changing the black hole mass, accretion rate or distance only changes the overall scaling of the spectrum; therefore, there is no effect on the shape of the spectrum or the spin estimates. We should note, however, that since the GRMHD simulations use dimensionless quantities, the gas mass scale in the simulations is arbitrary. Therefore, we have the ability to choose any accretion rate for a given disc thickness. For real discs, this is certainly not the case. The relation between the disc thickness and the luminosity is

Table 1. Spin estimates obtained by fitting the simulated spectra (for limb-darkened emission) with KERRBB, for a range of spins a_* and observer inclination angles i. The model identified as '1 loop' corresponds to a GRMHD simulation that has one poloidal magnetic loop in its initial disc configuration; all the other models have four loops arranged radially.

	$a_* = 0$ $\lvert h/r\rvert = 0.05$	$a_* = 0$, 1 loop $\lvert h/r\rvert = 0.07$	$a_* = 0.7$ $\lvert h/r\rvert = 0.04$
$i = 0^\circ$	0.08 ± 0.02	0.06 ± 0.01	0.71 ± 0.01
$i = 15^\circ$	0.08 ± 0.02	0.06 ± 0.01	0.72 ± 0.01
$i = 30^\circ$	0.09 ± 0.02	0.07 ± 0.02	0.72 ± 0.01
$i = 45^\circ$	0.10 ± 0.02	0.09 ± 0.02	0.73 ± 0.01
$i = 60^\circ$	0.11 ± 0.02	0.18 ± 0.01	0.76 ± 0.01
$i = 75^\circ$	0.15 ± 0.04	0.37 ± 0.01	0.80 ± 0.02

	$a_* = 0.9$ $\lvert h/r\rvert = 0.05$	$a_* = 0.98$ $\lvert h/r\rvert = 0.08$
$i = 0^\circ$	0.905 ± 0.002	0.985 ± 0.001
$i = 15^\circ$	0.906 ± 0.002	0.985 ± 0.001
$i = 30^\circ$	0.907 ± 0.003	0.985 ± 0.001
$i = 45^\circ$	0.908 ± 0.003	0.986 ± 0.001
$i = 60^\circ$	0.914 ± 0.005	0.987 ± 0.001
$i = 75^\circ$	0.929 ± 0.006	0.991 ± 0.001

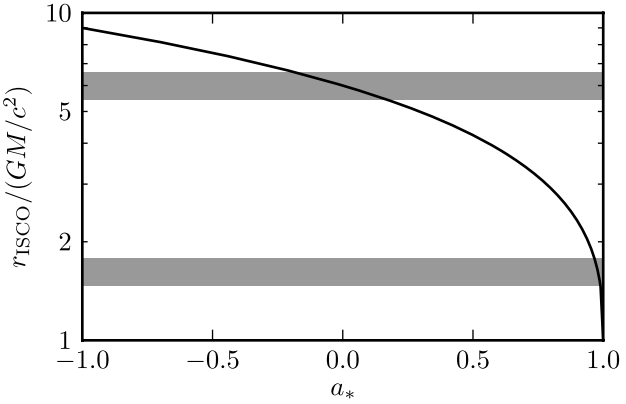

Figure 5. Relation between the black hole spin parameter a_* and the radius of the innermost stable circular orbit $r_{\rm ISCO}$.

[6] In addition, there are a couple of potential sources of systematic error: (i) our somewhat arbitrary choice of the matching radius used for extending the luminosity profiles beyond the inflow equilibrium radius (see Appendix A), and (ii) the fact that we restrict ourselves to the bound gas when calculating the luminosity profiles, as mentioned in footnote 4. We estimate the systematic error due to these two factors and, to be conservative, include them in quadrature in the error estimates that we quote in Tables 1 and 3.

[7] We also looked at spectra generated using isotropic emission. To fit these spectra we turned off the limb-darkening flag of KERRBB. The resulting spin estimates are very similar to those obtained using limb-darkened emission, so we do not show them here.

Table 2. Absolute and fractional errors in the estimated radius of the innermost stable circular orbit, $r_{\rm ISCO}$, corresponding to the spin estimates in Table 1.

	$a_* = 0$ $r_{\rm ISCO} = 6$	$a_* = 0.7$ $r_{\rm ISCO} = 3.39$
$i = 0^\circ$	−0.26 (−4.3 per cent)	−0.07 (−2.0 per cent)
$i = 15^\circ$	−0.27 (−4.5 per cent)	−0.07 (−2.2 per cent)
$i = 30^\circ$	−0.29 (−4.9 per cent)	−0.10 (−2.9 per cent)
$i = 45^\circ$	−0.33 (−5.4 per cent)	−0.15 (−4.5 per cent)
$i = 60^\circ$	−0.37 (−6.2 per cent)	−0.28 (−8.2 per cent)
$i = 75^\circ$	−0.49 (−8.2 per cent)	−0.51 (−15.1 per cent)
	$a_* = 0.9$ $r_{\rm ISCO} = 2.32$	$a_* = 0.98$ $r_{\rm ISCO} = 1.61$
$i = 0^\circ$	−0.04 (−1.6 per cent)	−0.07 (−4.1 per cent)
$i = 15^\circ$	−0.04 (−1.7 per cent)	−0.07 (−4.2 per cent)
$i = 30^\circ$	−0.04 (−1.9 per cent)	−0.07 (−4.5 per cent)
$i = 45^\circ$	−0.06 (−2.5 per cent)	−0.08 (−5.2 per cent)
$i = 60^\circ$	−0.10 (−4.1 per cent)	−0.11 (−6.9 per cent)
$i = 75^\circ$	−0.21 (−9.0 per cent)	−0.18 (−11.0 per cent)

Table 3. Fitted accretion rates for the cases in Table 1, in units of 10^{18} g s^{-1}. The input values in the GRMHD simulations are denoted by $\dot{M}_{\rm input}$.

	$a_* = 0$ $\dot{M}_{\rm input} = 2.45$	$a_* = 0.7$ $\dot{M}_{\rm input} = 1.35$
$i = 0^\circ$	2.46 ± 0.01	1.37 ± 0.01
$i = 15^\circ$	2.46 ± 0.01	1.37 ± 0.01
$i = 30^\circ$	2.46 ± 0.01	1.37 ± 0.01
$i = 45^\circ$	2.47 ± 0.01	1.36 ± 0.01
$i = 60^\circ$	2.48 ± 0.01	1.34 ± 0.02
$i = 75^\circ$	2.49 ± 0.04	1.30 ± 0.04
	$a_* = 0.9$ $\dot{M}_{\rm input} = 0.898$	$a_* = 0.98$ $\dot{M}_{\rm input} = 0.5982$
$i = 0^\circ$	0.901 ± 0.001	0.5983 ± 0.0003
$i = 15^\circ$	0.901 ± 0.001	0.5982 ± 0.0004
$i = 30^\circ$	0.902 ± 0.001	0.5983 ± 0.0005
$i = 45^\circ$	0.903 ± 0.001	0.5985 ± 0.0005
$i = 60^\circ$	0.904 ± 0.003	0.5980 ± 0.0008
$i = 75^\circ$	0.892 ± 0.007	0.594 ± 0.001

discussed in more detail in Section 3.1. We show there that the disc thicknesses used in our simulations ($|h/r| = 0.05$, 0.04, 0.05 and 0.08 for $a_* = 0$, 0.7, 0.9 and 0.98 respectively) correspond to $L/L_{\rm Edd} = 0.5, 0.4, 0.5$ and 0.7, respectively; therefore, strictly speaking, our estimates of the errors in the spin determination are only applicable for these luminosities.

We carried out a test run at $a_* = 0$ with a different initial magnetic field configuration that has one poloidal loop instead of four as in our other runs. This model is closer in spirit to the simulations run by Noble et al. (2009, 2010). We find that the one-loop model gives hotter spectra and a larger error in the derived value of the spin at large inclination angles (compare the first two columns of Table 1). This agrees with the results described by Noble et al. (2010) and Penna et al. (2010), who investigated the behaviour of other diagnostics such as the angular momentum and shear stress and showed that GRMHD discs calculated from single-loop initial conditions generally deviate more strongly from the NT model compared to discs obtained from multi-loop initial conditions. Penna et al. (2010) argued that the multi-loop case is more natural since it better mimics disc turbulence, whereas the one-loop case might introduce an artificial long-range radial coherence in the solution.

Table 4. Spin estimates from spectra obtained by excluding the plunging region and setting the four-velocity in the disc to its NT value (second column) compared with the original spin estimates from Table 1 (third column).

$a_* = 0.9$, $i = 75^\circ$	0.92	0.93
$a_* = 0.9$, $i = 45^\circ$	0.91	0.91
$a_* = 0$, $i = 75^\circ$	0.13	0.15

The errors in the spin estimates could be due to a number of reasons: (1) The disc emissivity profile outside the ISCO is different in the simulations compared to the NT model, as Fig. 1 shows; (2) the simulations have some radiation coming from the plunging region inside the ISCO and (3) even outside the plunging region, the radial component of the gas four-velocity is not negligible. To find out which of these is the dominant effect, we calculated some spectra from the simulated discs by excluding the region inside the ISCO and setting the gas velocity outside the ISCO to its NT value. Any residual differences in the spin estimates would solely be due to (1).

The results are shown in Table 4. We see that spin estimates obtained from the GRMHD simulations are still significantly different from the true values. This shows that the dominant reason for the errors in the spin estimates is the fact that, even outside the ISCO, the disc emissivity profile in the simulations is different from the NT profile; more specifically, that the peak of the profile is shifted to smaller radii, as mentioned in Section 2. We should note, however, that for discs thicker than those considered in this work by about a factor of 2 or more, the effect of the plunging region is important. This follows from the finding of Penna et al. (2010) that deviations of the GRMHD simulations from the NT model increase with increasing disc thickness.

3.1 Effective accretion rates of the GRMHD models

The GRMHD models that we have used in this study make use of dimensionless quantities and do not include detailed radiation transfer. Hence there is no direct way of estimating the physical mass accretion rate (g s^{-1}) or the true radiative luminosity (erg s^{-1}) of the models. To estimate these quantities, we use an indirect method in which we compare the vertical thicknesses of the simulated discs against physical disc models that do include radiation transfer and radiation pressure and solve for the vertical disc structure.

We use two models for this comparison. One is a semi-analytical model of a slim disc (Sądowski et al. 2011) which goes beyond the NT model by including the effect of energy advection in the radial equations. At each radius r, the model solves the condition of vertical hydrostatic equilibrium and includes radiative transfer approximately. The other model (Davis et al. 2005) assumes the NT model for the radial structure but carries out a careful and detailed computation of radiation transfer, including non-local thermodynamic equilibrium effects, at each r. This model is identical to the XSPEC model BHSPEC (Davis & Hubeny 2006). Each of these models treats some part of the physics very well, but neither has all the ingredients one would like to include, viz. advection, full radiative

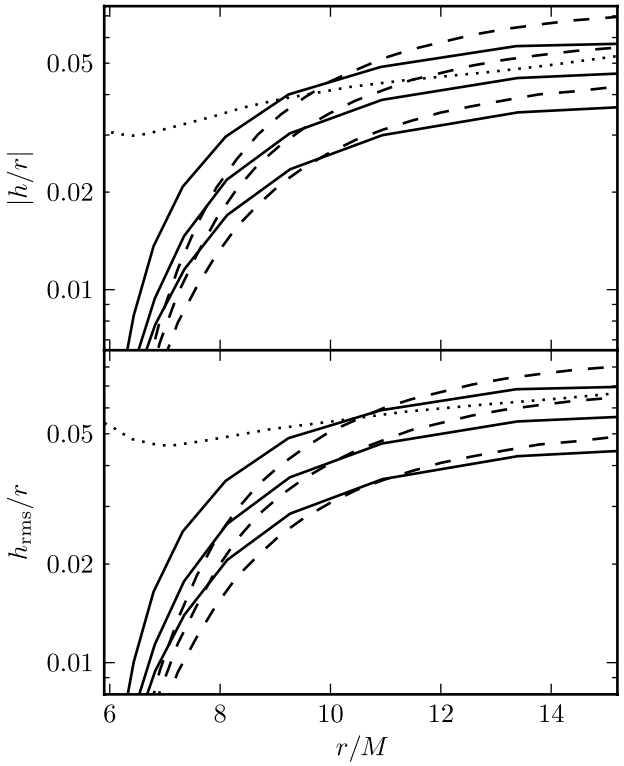

Figure 6. Profiles of $|h/r|$ for $a_* = 0$ from the slim-disc model of Sądowski et al. (2011) (solid lines) and the detailed radiative transfer model BHSPEC of Davis & Hubeny (2006) (dashed lines) for luminosities $L/L_{\rm Edd} = 0.3$, 0.4, 0.5 (bottom to top in each panel), compared with the profile obtained from the GRMHD simulation (dotted lines). The top panel shows the density scaleheight $|h| = \int \rho\,|z|\,{\rm d}z / \int \rho\,{\rm d}z$, while the bottom panel shows the rms height $h_{\rm rms} = (\int \rho\, z^2\,{\rm d}z / \int \rho\,{\rm d}z)^{1/2}$.

transfer, magnetic fields, deviations from hydrostatic equilibrium, self-irradiation, etc.

Fig. 6 shows the disc thickness as a function of r for $a_* = 0$, as predicted by the slim-disc model (solid lines, corresponding to $L/L_{\rm Edd} = 0.3$, 0.4, 0.5, bottom to top) and BHSPEC (dashed lines, same set of luminosities). These curves should be compared with the disc thickness in the GRMHD simulation (dotted lines). The top panel shows the density scaleheight $|h| = \int \rho\,|z|\,{\rm d}z / \int \rho\,{\rm d}z$, while the bottom panel shows the rms height $h_{\rm rms} = (\int \rho\, z^2\,{\rm d}z / \int \rho\,{\rm d}z)^{1/2}$.

At radii close to the ISCO, the slim disc and BHSPEC models indicate that the disc thickness plunges to small values, whereas the GRMHD simulation shows a much smaller decrease. We believe there are at least three reasons for this discrepancy: (i) the GRMHD simulations cool the gas by forcing it towards a constant entropy, which may not be justified in the plunging region; (ii) the simulated GRMHD disc includes magnetic fields whose pressure provides additional support in the vertical direction, whereas the other two models do not and (iii) the simulated disc begins to deviate from hydrostatic equilibrium as the radial velocity becomes large near the ISCO and the gas has less time to reach equilibrium, whereas the other models hardwire the condition of hydrostatic equilibrium at all radii. We estimate that the last two are only important well inside the ISCO, however, while the discrepancy sets in already at larger radii. These are interesting issues which we hope to explore in the future. For the purposes of this section, we simply ignore the region of the simulation near the ISCO.

Table 5. Spin estimates for $a_* = 0$ from GRMHD simulations of a thicker disc ($|h/r| = 0.09$) compared with those for the thinner ($|h/r| = 0.05$) disc shown in Table 1.

$\lvert h/r\rvert$	$L/L_{\rm Edd}$	$i = 15^\circ$	$i = 45^\circ$	$i = 75^\circ$
0.05	0.5	0.08	0.10	0.15
0.09	0.9	0.08	0.19	0.50

For the comparisons described here, we select a radius of $r = 12M = 2r_{\rm ISCO}$, which is well outside the ISCO, and determine the luminosities at which the slim disc and BHSPEC models give the same disc thickness as we obtain in the simulated disc. We see from Fig. 6 that the thickness measure $|h/r| \sim 0.05$ in the simulated GRMHD disc corresponds to $L/L_{\rm Edd} \sim 0.5$ according to the slim-disc model and $\sim$0.4 according to BHSPEC. A comparison of the thickness measure $h_{\rm rms}/r$ gives slightly larger values of $L/L_{\rm Edd}$. Similar analysis (again at $r = 2r_{\rm ISCO}$) for $a_* = 0.7$, 0.9 and 0.98 shows that $L/L_{\rm Edd} \sim 0.4$, 0.5 and 0.7 respectively according to the slim-disc model, and 0.4, 0.4 and 0.6 respectively according to BHSPEC.

The above luminosities are much higher than the typical luminosities ($L/L_{\rm Edd} < 0.3$) at which black hole binary spectra are analysed for spin determination using the continuum-fitting method (from Fig. 6, this corresponds to $|h/r| \lesssim 0.03$). Therefore, the errors in the spin determination quoted in Section 3 are not directly applicable to observations. At lower luminosities, the accretion disc would be thinner, as Fig. 6 shows. Due to computational resource requirements, it is not currently possible for us to perform GRMHD simulations for discs thinner than those presented here. What we can do instead is to scale the results from the simulations to more realistic thinner discs at lower luminosities. Table 5 compares the spins obtained from two GRMHD simulations corresponding to $a_* = 0$, one with $|h/r| = 0.05$ (which we have focused on so far) and another with $|h/r| = 0.09$. We see that the error in the spin estimate is much larger for the latter model. Thus, it is clear that at the lower luminosities that are interesting from an observational point of view, the errors in the spin estimates would be significantly smaller than those in Table 1.

As an aside, we note that McClintock et al. (2006) calculated the height of the disc photosphere as a function of radius for an NT disc (see fig. 17 in their paper). The disc heights they quote are larger than the density scaleheights shown in Fig. 6 by roughly a factor of 2–3. We have calculated the location of the photosphere corresponding to the slim disc and BHSPEC models, and find that they agree fairly well with the values obtained by McClintock et al. (2006).

3.2 Effect of a finite photospheric height

So far we have been calculating spectra using equatorial profiles of the emitted flux $F(r)$ and the fluid four velocity $u^\mu(r)$, which are obtained, as mentioned in Section 2, by vertically integrating the GRMHD simulated disc structure. This integration effectively collapses the disc into the equatorial plane, which is where the disc emission is assumed to originate from. The errors in the spin estimates quoted above have therefore been purely due to the departure of the equatorial flux and fluid velocity from their NT values. In reality, however, the observed disc emission comes from the photosphere, which is at a finite height above the equatorial plane. The effect of this on the spin estimates needs to be checked.

Table 6. Spin estimates from spectra calculated using a finite photospheric height for the disc ($|h_{\rm phot}/r| = 0.2$) for both NT and simulated disc temperature profiles, at selected values of spin and inclination.

	NT disc	Simulated disc	Simulated disc (original estimates from Table 1)
$a_* = 0.9, i = 75^\circ$	0.88	0.90	0.93
$a_* = 0.9, i = 45^\circ$	0.89	0.90	0.91
$a_* = 0, i = 75^\circ$	−0.05	0.09	0.15

The method we use for doing this is very crude; our only goal here is to find out whether or not this effect could be important. The slim disc and BHSPEC models mentioned above, and the calculations of McClintock et al. (2006), show that the photosphere height is about 2–3 scaleheights. Since we want to see how large the effect of off-mid-plane emission could possibly be, we choose a larger photosphere height: $h_{\rm phot}/r \sim 4|h/r|$, where $|h/r|$ is the disc half-thickness measured at one scaleheight above the disc mid-plane. We then repeat our ray-tracing computation, but following the geodesics until they hit the photosphere instead of the equatorial plane [the photosphere as defined above corresponds to $\theta = \pi/2 - \delta$, where $\delta = \tan^{-1}(h_{\rm phot}/r)$]. Finally, we assume that the flux and gas four-velocity profiles at the point of emission are given by their equatorial values $F(r)$ and $u^\mu(r)$, enabling us to calculate the spectra. Table 6 indicates that the effect on the estimates of a_* may be significant at high spins. However, it is encouraging to note that the errors in the spin estimates decrease when we use a finite photospheric height.

We should also note that Li et al. (2010) find a much larger effect on the spin estimates when they take the effect of a finite photospheric height into account. We believe this is due to the fact that the $|h/r|$ profile in their analysis drops relatively sharply at small radii, like the profiles from the slim disc model and BHSPEC shown in Fig. 6. This disc geometry leads to self-shadowing of the disc. For our analysis in this subsection, on the other hand, we have chosen a constant $|h/r|$. Even if we were to use the $|h/r|$ profile from the GRMHD simulations, we would not expect to see significant self-shadowing, since the $|h/r|$ profile in the simulated model is nearly constant with radius (Fig. 6).

4 A COMPARISON OF OBSERVATIONAL AND MODEL-DEPENDENT ERRORS

The obvious question at this point is how big the errors in the spin estimates listed in Table 1 are compared with the observational uncertainties in spin determination. We address this question in this section. The spins of eight stellar mass black holes have been measured so far using the continuum-fitting method. The observational error estimates for the first four (see Shafee et al. 2006 for GRO J1655−40 and 4U 1543−47, Davis et al. 2006 for LMC X-3 and McClintock et al. 2006 for GRS 1915+105) are very approximate, and we disregard these results here. In more recent work, the principal sources of observational errors, as well as the uncertainties in the key model parameters (e.g. the viscosity parameter α), have been treated in detail. Moreover, in a recent paper on XTE J1550−564, Steiner et al. (2010b) have exhaustively explored many additional sources of error (see their table 3 and Appendix A). The upshot of the work to date is that in every case the uncertainty in a_* is completely dominated by the errors in three key dynamical parameters that are input when fitting the X-ray spectral data (McClintock et al. 2006). These parameters are the distance D, the black hole mass M and the inclination of the inner disc i (which is assumed to be aligned with the orbital angular momentum vector of the binary; Li, Narayan & McClintock 2009). In order to determine the error in a_* due to the combined uncertainties in D, M and i, Monte Carlo simulations are performed assuming that these parameters are normally and independently distributed (e.g. Gou et al. 2009).

Table 7 gives selected observational data for four black holes (all of these have been subjected to the rigorous error analysis described above): the inclination angle, which has an important effect on the model results (Tables 1–6); the spin parameter; the absolute and fractional errors in $r_{\rm ISCO}$ (compare Table 2); and the luminosity. All errors are quoted at the 68 per cent level of confidence. Note that the values of a_* range widely from ∼0 to ∼0.9. As a rough characterization, the uncertainties in the values of a_* are $\Delta a_* \sim \pm 0.05$ for the rapidly spinning pair of black holes and $\Delta a_* \sim \pm 0.2$ for the slowly spinning pair. The corresponding fractional errors in $r_{\rm ISCO}$ range from approximately 10 to 20 per cent. Comparing the fractional errors in $r_{\rm ISCO}$ in Table 7 with the closest counterpart results in Table 2 (i.e. closest matches for i and a_*), we find that the error in the NT model is in all cases less than the observational error: A0620−00, 5.4 versus 11.5 per cent; XTE J1550−564, 8.2 versus 17.9 per cent; M33 X-7, 9.0 versus 10.7 per cent and LMC X-1, 1.9 versus 20.5 per cent.

Furthermore, the estimates of the modelling error due to deviations from the NT model obtained in this paper are very likely overestimates because the GRMHD simulation results necessarily correspond to relatively luminous discs: $L/L_{\rm Edd} = 0.4 - 0.7$, whereas the observed luminosities are typically only $L/L_{\rm Edd} \sim 0.15$ (Table 7) and are strictly limited to $L/L_{\rm Edd} < 0.30$ (McClintock et al. 2006). Because the NT model improves as the thickness and luminosity of the disc decrease (Table 5), *we conclude that use of the NT thin-disc model does not limit our accuracy. Rather, it is the uncertainties in the input parameters D, M* and *i that strongly dominate the error in* a_*.

5 CONCLUSIONS AND DISCUSSION

The main conclusion of this paper is that observational errors in current measurements of black hole spin by the continuum-fitting method dominate over the errors incurred by using the idealized

Table 7. Data for four black holes. The entries are the number of spectra analysed, inclination angle, spin parameter, the approximate/symmetrized absolute and fractional errors in $r_{\rm ISCO}$, and the Eddington-scaled luminosity.

Black Hole	No.	i (°)	a_*	$\Delta r(\Delta r/r)$	$L/L_{\rm Edd}$	Reference
A0620–00	1	51.0 ± 0.9	0.12 ± 0.19	±0.65(11.5 per cent)	0.11	Gou et al. (2010)
XTE J1550−564	45[a]	74.7 ± 3.8	$0.34^{+0.20}_{-0.28}$	±0.86(17.9 per cent)	0.05–0.30	Steiner et al. (2010b)
M33 X-7	15	74.6 ± 1.0	0.84 ± 0.05	±0.29(10.7 per cent)	0.07–0.11	Liu et al. (2008, 2010)
LMC X-1	18	36.4 ± 2.0	$0.92^{+0.05}_{-0.07}$	±0.43(20.5 per cent)	0.15–0.17	Gou et al. (2009)

[a] Typical value: number of spectra analysed varies depending on details of data selection (see Steiner et al. 2010b).

NT model. We reached this conclusion by using 3D GRMHD simulations of thin discs to obtain realistic disc temperature profiles, then calculating the corresponding spectra, and finally fitting these spectra using the standard XSPEC model KERRBB. For disc thicknesses $|h/r| \sim 0.04$–0.08, the errors in a_* are up to about 0.2, depending on the inclination, for a non-spinning black hole, and up to about 0.1, 0.03 and 0.01 for black holes with spins of 0.7, 0.9 and 0.98, respectively (Table 1). The errors in the spin estimates are particularly large at low spins and high inclinations, e.g. we find a spin estimate of 0.15 for a non-spinning black hole viewed at an inclination angle of 75°. The results are quite close to those obtained by Reynolds & Fabian (2008) for the iron line fitting method (see fig. 5 of their paper). Interestingly, we find that the fitted accretion rates are correct to within a few per cent.

A new and important contribution in this paper is that we establish via the slim-disc and BHSPEC models an approximate correspondence between the disc thickness as calculated from GRMHD simulations (Section 2.1) and the key disc observable $L/L_{\rm Edd}$ (Section 3.1). Even though the simulated discs considered in this paper are geometrically quite thin, $|h/r| \sim 0.04$–0.08, nevertheless it turns out that such discs correspond to fairly high luminosities, $L/L_{\rm Edd} \sim 0.4$–0.7. For comparison, in observational work based on the continuum-fitting method, the data-selection criterion $L/L_{\rm Edd} < 0.3$ (McClintock et al. 2006) is generally employed (which, from Fig. 6, corresponds to $|h/r| \lesssim 0.03$). The validity and usefulness of this criterion can be best judged by examining the results for 411 observations of LMC X-3 in Steiner et al. (2010a, see their figs 2 and 3). For $L/L_{\rm Edd} < 0.3$, the inner disc radius $r_{\rm in}$ is very nearly constant, rising only slightly at luminosities above $L/L_{\rm Edd} \approx 0.2$. However, $r_{\rm in}$ increases quite abruptly as the luminosity exceeds 30 per cent of Eddington. Remarkably, at these higher luminosities there is little scatter in the data and the increase in $r_{\rm in}$ is smooth and systematic.

It is difficult to say at this stage what the reason is for the above increase in the inner disc radius above the critical luminosity of $\sim 0.3 L_{\rm Edd}$. Both the GRMHD and the slim-disc models predict that the inner disc radius should decrease (see the discussion of the radiation edge in Abramowicz et al. 2010).[8] On the other hand, Li et al. (2010) were able to reproduce the observed increase by considering self-shadowing of the disc as a result of the off-midplane location of the disc photosphere. Interestingly, Abramowicz et al. (2010) find that the inner radius of the disc is fairly close to the NT value for luminosities $L \lesssim 0.3 L_{\rm Edd}$, and that the inner edge decreases quite abruptly at higher values of $\dot{M}$. This, combined with the observed behaviour of $r_{\rm in}$ in LMC X-3, may be a hint that something qualitatively different happens at $L/L_{\rm Edd} \approx 0.3$; perhaps energy advection or disc self-shadowing becomes suddenly more relevant.

One firm conclusion can be drawn from the results presented in this paper. Since Table 5 indicates that the modelling error decreases as the disc thickness decreases, whatever the behaviour of $r_{\rm in}$ may be above $L/L_{\rm Edd} \approx 0.3$, at luminosities appropriate to the continuum-fitting method ($L < 0.3 L_{\rm Edd}$), where the disc will be geometrically very thin, the errors in the spin estimates will be even smaller than those quoted in Table 1. Therefore, these errors are not a concern for the continuum-fitting method of measuring black hole spin.

[8] The caveat, as Abramowicz et al. (2010) point out, is that there are various ways of defining the inner edge of the accretion disc, and for some definitions, the inner disc radius can increase when the luminosity increases beyond $\sim 0.3 L_{\rm Edd}$ if the viscosity parameter is large enough ($\alpha \gtrsim 0.2$). However, the values of α that we see in our simulations are smaller, so this caveat does not present any problem.

We must note one caveat about comparing the density scaleheight from the GRMHD simulations with that from the slim-disc and BHSPEC models: the latter models do not include magnetic pressure. The increase in the photosphere height due to magnetic pressure could be as large as a factor of 2 (Hirose, Krolik & Stone 2006), although other studies have found more modest changes (Blaes et al. 2006; Davis et al. 2009).

ACKNOWLEDGMENTS

The authors wish to thank Jason Dexter for a critical reading of the manuscript, and the referee for several comments that helped improve the paper. This work was supported by NASA grant NNX08AH32G and NSF grant AST-0805832. The simulations presented in this work were performed using resources provided by the NASA High-End Computing (HEC) Program through the NASA Advanced Supercomputing (NAS) Division at Ames Research Center, and TeraGrid resources provided by the National Institute for Computational Sciences (NICS).

REFERENCES

Abramowitz M., Stegun I. A., 1972, in Abramowitz M., Stegun I. A., eds, Handbook of Mathematical Functions. Dover, New York
Abramowicz M. A., Jaroszyński M., Kato S., Lasota J., Różańska A., Sądowski A., 2010, A&A, 521, A15
Afshordi N., Paczyński B., 2003, ApJ, 592, 354
Arnaud K. A., 1996, in Jacoby G. H., Barnes J., eds, ASP Conf. Ser. Vol. 101, Astronomical Data Analysis Software and Systems V. Astron. Soc. Pac., San Francisco, p. 17
Beckwith K., Hawley J. F., Krolik J. H., 2008, MNRAS, 390, 21
Blaes O. M., Davis S. W., Hirose S., Krolik J. H., Stone J. M., 2006, ApJ, 645, 1402
Brenneman L. W., Reynolds C. S., 2006, ApJ, 652, 1028
Cunningham C. T., 1975, ApJ, 202, 788
Cunningham C. T., Bardeen J. M., 1973, ApJ, 183, 237
Davis S. W., Hubeny I., 2006, ApJS, 164, 530
Davis S. W., Blaes O. M., Hubeny I., Turner N. J., 2005, ApJ, 621, 372
Davis S. W., Done C., Blaes O. M., 2006, ApJ, 647, 525
Davis S. W., Blaes O. M., Hirose S., Krolik J. H., 2009, ApJ, 703, 569
De Villiers J., Hawley J. F., Krolik J. H., 2003, ApJ, 599, 1238
Dexter J., Agol E., 2009, ApJ, 696, 1616
Fabian A. C., Rees M. J., Stella L., White N. E., 1989, MNRAS, 238, 729
Fabian A. C., Iwasawa K., Reynolds C. S., Young A. J., 2000, PASP, 112, 1145
Frank J., King A., Raine D. J., 2002, in Frank J., King A., Raine D. J., eds, Accretion Power in Astrophysics, 3rd edn. Cambridge Univ. Press, Cambridge
Gammie C. F., McKinney J. C., Tóth G., 2003, ApJ, 589, 444
Gou L. et al., 2009, ApJ, 701, 1076
Gou L., McClintock J. E., Steiner J. F., Narayan R., Cantrell A. G., Bailyn C. D., Orosz J. A., 2010, ApJ, 718, L122
Hameury J., Marck J., Pelat D., 1994, A&A, 287, 795
Hirose S., Krolik J. H., Stone J. M., 2006, ApJ, 640, 901
Krolik J. H., 1999, ApJ, 515, L73
Laor A., 1991, ApJ, 376, 90
Li L., Zimmerman E. R., Narayan R., McClintock J. E., 2005, ApJS, 157, 335
Li L., Narayan R., McClintock J. E., 2009, ApJ, 691, 847
Li G., Yuan Y., Cao X., 2010, ApJ, 715, 623
Liu J., McClintock J. E., Narayan R., Davis S. W., Orosz J. A., 2008, ApJ, 679, L37
Liu J., McClintock J. E., Narayan R., Davis S. W., Orosz J. A., 2010, ApJ, 719, L109
McClintock J. E., Shafee R., Narayan R., Remillard R. A., Davis S. W., Li L., 2006, ApJ, 652, 518

McKinney J. C., 2006, MNRAS, 368, 1561
McKinney J. C., Blandford R. D., 2009, MNRAS, 394, L126
Marck J., 1996, Class. Quantum Grav., 13, 393
Narayan R., McClintock J. E., Shafee R., 2008, in Yuan Y. F., Li X. D., Lai D., eds, AIP Conf. Ser. 968, Astrophysics of Compact Objects. Am. Inst. Phys., New York, p. 265
Noble S. C., Krolik J. H., Hawley J. F., 2009, ApJ, 692, 411
Noble S. C., Krolik J. H., Hawley J. F., 2010, ApJ, 711, 959
Novikov I. D., Thorne K. S., 1973, in Dewitt C., Dewitt B. S., eds, Black Holes (Les Astres Occlus). Gordon and Breach, Paris, p. 343 (NT)
Paczyński B., 2000 (arXiv:astro-ph/0004129)
Page D. N., Thorne K. S., 1974, ApJ, 191, 499 (PT)
Penna R. F., McKinney J. C., Narayan R., Tchekhovskoy A., Shafee R., McClintock J. E., 2010, MNRAS, 408, 752
Reynolds C. S., Fabian A. C., 2008, ApJ, 675, 1048
Reynolds C. S., Nowak M. A., 2003, Phys. Rep., 377, 389
Sądowski A., 2009, ApJS, 183, 171
Sądowski A., Abramowicz M., Bursa M., Kluźniak W., Lasota J., Rozanska A., 2011, A&A, 527, A17
Shafee R., McClintock J. E., Narayan R., Davis S. W., Li L., Remillard R. A., 2006, ApJ, 636, L113
Shafee R., McKinney J. C., Narayan R., Tchekhovskoy A., Gammie C. F., McClintock J. E., 2008a, ApJ, 687, L25
Shafee R., Narayan R., McClintock J. E., 2008b, ApJ, 676, 549
Shakura N. I., Sunyaev R. A., 1973, A&A, 24, 337
Shapiro S. L., Teukolsky S. A., 1983, in Shapiro S. L., Teukolsky S. A., eds, Black Holes, White Dwarfs, and Neutron Stars: The Physics of Compact Objects. Wiley, New York, p. 362.
Shcherbakov R. V., Huang L., 2011, MNRAS, 410, 1052
Shcherbakov R. V., Penna R. F., McKinney J. C., 2010, ApJ, submitted (arXiv:1007.4832)
Shimura T., Takahara F., 1995, ApJ, 445, 780
Steiner J. F., McClintock J. E., Remillard R. A., Narayan R., Gou L., 2009, ApJ, 701, L83
Steiner J. F., McClintock J. E., Remillard R. A., Gou L., Yamada S., Narayan R., 2010a, ApJ, 718, L117
Steiner J. F. et al., 2010b preprint (arXiv:1010.1013)
Zhang S. N., Cui W., Chen W., 1997, ApJ, 482, L155

APPENDIX A: MATCHING A GRMHD MODEL TO THE PAGE AND THORNE SOLUTION

Page & Thorne (1974, hereafter PT) define in their equations (31a,b) two quantities: (i) $f(r)$, which is proportional to the local disc flux $F_{\rm com}(r)$ emitted from one side of the disc, as measured in the co-moving frame of the fluid,[9] and (ii) $w(r)$, which is proportional to the shear stress W^r_ϕ:

$$f(r) = 4\pi r F_{\rm com}/\dot{M}, \tag{A1}$$

$$w(r) = 2\pi r W^r_\phi/\dot{M}. \tag{A2}$$

These quantities enter the angular momentum and energy conservation laws via (see PT, equations 32a,b)

$$(L^\dagger - w)_{,r} = fL^\dagger, \tag{A3}$$

$$(E^\dagger - \Omega w)_{,r} = fE^\dagger, \tag{A4}$$

where $L^\dagger(r)$, $E^\dagger(r)$ and $\Omega(r)$ are the specific angular momentum, specific energy-at-infinity and the angular velocity. Equations (A3) and (A4) lead to the further relation (PT, equation 33):

$$f = -\Omega_{,r}(E^\dagger - \Omega L^\dagger)^{-1} w. \tag{A5}$$

[9] The procedure for transforming the flux between the BL and comoving frames is described in Appendix B2.

For a thin accretion disc, PT show that f has a general solution of the form:

$$f(r) = -\Omega_{,r}(E^\dagger - \Omega L^\dagger)^{-2}\left[\int (E^\dagger - \Omega L^\dagger)L^\dagger_{,r}{\rm d}r + C\right], \tag{A6}$$

where C is an integration constant. They assume that the stress vanishes at the ISCO, and thereby determine the value of C. They then obtain the following particular solution:

$$f_{\rm PT}(r) = -\Omega_{,r}(E^\dagger - \Omega L^\dagger)^{-2}\int_{r_{\rm ISCO}}^{r} (E^\dagger - \Omega L^\dagger)L^\dagger_{,r}{\rm d}r. \tag{A7}$$

Equation (15n) in PT gives an explicit analytical expression for $f_{\rm PT}(r)$.

We are interested in the following more general problem. We have a GRMHD numerical solution of a thin disc that has reached inflow equilibrium out to some radius $r_{\rm ie}$ (defined in Penna et al. 2010). Beyond this radius, however, we cannot trust the numerical results, so we would like to match our simulation model to the PT solution. This will allow us to extrapolate the simulation beyond $r_{\rm ie}$ and even beyond the radial range of the numerical grid. We wish to avoid the particular solution $f_{\rm PT}$ given above since that assumes zero stress at the ISCO. Instead, we fit for the value of the integration constant C using the simulation. We also redefine the constant C slightly so that the fitting is made at $r_{\rm ie}$ rather than $r_{\rm ISCO}$.

Let us write equation (A6) as follows,

$$f(r) = -\Omega_{,r}(E^\dagger - \Omega L^\dagger)^{-2}\left[\int_{r_{\rm ie}}^{r} (E^\dagger - \Omega L^\dagger)L^\dagger_{,r}{\rm d}r + C\right], \quad r \geq r_{\rm ie}, \tag{A8}$$

where the new constant C is to be determined from the simulation at $r = r_{\rm ie}$. We can write

$$\int_{r_{\rm ie}}^{r} (E^\dagger - \Omega L^\dagger)L^\dagger_{,r}{\rm d}r = \int_{r_{\rm ISCO}}^{r} (E^\dagger - \Omega L^\dagger)L^\dagger_{,r}{\rm d}r - \int_{r_{\rm ISCO}}^{r_{\rm ie}} (E^\dagger - \Omega L^\dagger)L^\dagger_{,r}{\rm d}r \tag{A9}$$

$$= \left[\frac{(E^\dagger - \Omega L^\dagger)^2}{-\Omega_{,r}}\right]_r f_{\rm PT}(r) - \left[\frac{(E^\dagger - \Omega L^\dagger)^2}{-\Omega_{,r}}\right]_{r_{\rm ie}} f_{\rm PT}(r_{\rm ie}). \tag{A10}$$

Substituting in equation (A8), we obtain the result we seek:

$$f(r) = f_{\rm PT}(r) - \frac{[(E^\dagger - \Omega L^\dagger)^2/\Omega_{,r}]_{r_{\rm ie}}}{[(E^\dagger - \Omega L^\dagger)^2/\Omega_{,r}]_r} f_{\rm PT}(r_{\rm ie}) - \frac{\Omega_{,r}}{(E^\dagger - \Omega L^\dagger)^2} C, \quad r \geq r_{\rm ie}, \tag{A11}$$

where

$$C = -\left[\frac{(E^\dagger - \Omega L^\dagger)^2}{\Omega_{,r}}\right]_{r_{\rm ie}} 4\pi r_{\rm ie} F_{\rm com}(r_{\rm ie})/\dot{M}. \tag{A12}$$

Except for $F_{\rm com}(r_{\rm ie})/\dot{M}$, the local disc flux of the simulation at $r = r_{\rm ie}$, all the other quantities are obtained from the idealized PT model and can be evaluated at any r outside the matching radius $r_{\rm ie}$. With this matching procedure, the local disc flux from the converged region of the simulation can be extrapolated to arbitrary radii.

The choice of the matching radius $r_{\rm ie}$ is an important issue. We would like to use as large a radius as possible, while still staying within the inflow equilibrium radius, but we need to ensure that the

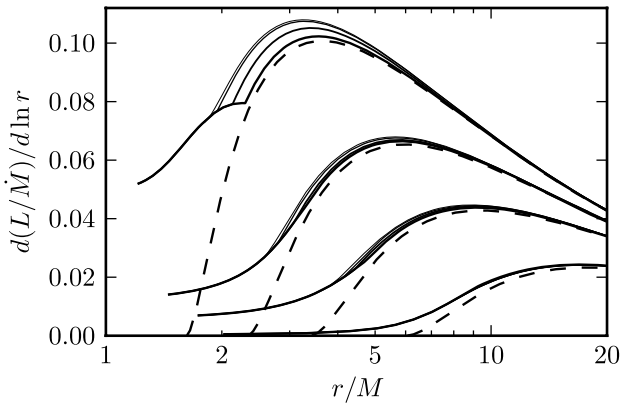

Figure A1. Similar figure to Fig. 1, except that the solid line for each spin in Fig. 1 is replaced by a cluster of solid lines showing the luminosity profiles for different values of the matching radius, $r_{\rm ie}/r_{\rm ISCO} = 1.1$, 1.2, 1.3, 1.4 (solid lines, top to bottom).

choice of the matching radius does not affect the luminosity profiles $\mathrm{d}(L/\dot{M})/\mathrm{d}(\ln r)$ significantly. Fig. A1 shows the luminosity profiles for $a_* = 0$, 0.7, 0.9 and 0.98 (bottom to top). For each spin, the cluster of solid lines shows the luminosity profiles for $r_{\rm ie}/r_{\rm ISCO} = 1.1$, 1.2, 1.3, 1.4, and the dashed line shows the NT profile. It is clear that for all the models except $a_* = 0.98$, the choice of the matching radius has little effect on the luminosity profiles. This turns out to be particularly true for $r_{\rm ie}/r_{\rm ISCO} < 1.3$, as a closer look reveals. We therefore use $r_{\rm ie} = 1.3 r_{\rm ISCO}$ in those three models. The $a_* = 0.98$ model, however, did not attain inflow equilibrium out to a sufficiently large radius. Its luminosity profiles therefore show more sensitivity to the matching radius. Hence we choose $r_{\rm ie} = 1.2 r_{\rm ISCO}$ for this model. This is a conservative choice, since it results in a larger deviation from the NT luminosity. The predicted errors in the spin estimates shown for this model in Table 1 are therefore likely to be overestimates.

APPENDIX B: TRANSFORMATION BETWEEN THE BOYER–LINDQUIST AND COMOVING FRAMES

B1 Transformation of vectors and one-forms

To transform the four-momentum, we need to find the orthonormal basis of the comoving frame, which we do using the Gram–Schmidt orthonormalization procedure as described in Beckwith, Hawley & Krolik (2008) and Shcherbakov & Huang (2011). Let us denote the comoving-frame basis vectors by $e_{(\nu)}$ and the fluid four-velocity by u^μ. In the comoving frame, since the fluid is at rest, its four-velocity u is equal to $e_{(t)}$. This is a coordinate-independent statement; it is true in any frame. We can thus denote the components of the $e_{(\nu)}$ in the BL frame by

$$\begin{aligned} e^\mu_{(t)} &= u^\mu = (u^t, u^r, u^\theta, u^\phi), \\ e^\mu_{(r)} &= (\lambda_3, \lambda_4, 0, \lambda_5), \\ e^\mu_{(\theta)} &= (\lambda_6, \lambda_7, \lambda_8, \lambda_9), \\ e^\mu_{(\phi)} &= (\lambda_1, 0, 0, \lambda_2), \end{aligned} \tag{B1}$$

where the λ_i are determined by imposing orthonormality, i.e. that $e^\mu_{(\nu)} e^{(\psi)}_\mu = \delta^{(\psi)}_{(\nu)}$. (The index μ in $e^\mu_{(\nu)}$ is lowered using the BL metric $g_{\alpha\beta}$, while the index (ν) is raised using the Minkowski metric $\eta^{(\alpha)(\beta)} = \mathrm{diag}(-1, 1, 1, 1)$, since we want the comoving frame to be locally flat as well.) The $e^\mu_{(\nu)}$ are the components of the transformation matrix for four-vector components from the comoving frame into the BL frame. Some algebra gives

$$\begin{aligned} e^\mu_{(t)} &= (u^t, u^r, u^\theta, u^\phi), \\ e^\mu_{(r)} &= (u_r u^t, -(u_t u^t + u_\phi u^\phi), 0, u_r u^\phi)/N_r, \\ e^\mu_{(\theta)} &= (u_\theta u^t, u_\theta u^r, 1 + u_\theta u^\theta, u_\theta u^\phi)/N_\theta, \\ e^\mu_{(\phi)} &= (u_\phi, 0, 0, -u_t)/N_\phi, \end{aligned}$$

and its inverse

$$\begin{aligned} e^{(t)}_\mu &= (-u_t, -u_r, -u_\theta, -u_\phi), \\ e^{(r)}_\mu &= (u_r u_t, -g_{rr}(u_t u^t + u_\phi u^\phi), 0, u_r u_\phi)/N_r, \\ e^{(\theta)}_\mu &= (u_\theta u_t, u_\theta u_r, g_{\theta\theta}(1 + u_\theta u^\theta), u_\theta u_\phi)/N_\theta, \\ e^{(\phi)}_\mu &= -\Delta \sin^2\theta (u^\phi, 0, 0, -u^t)/N_\phi, \end{aligned}$$

with

$$\begin{aligned} N_r^2 &= -g_{rr}(u_t u^t + u_\phi u^\phi)(1 + u_\theta u^\theta) \\ N_\theta^2 &= g_{\theta\theta}(1 + u_\theta u^\theta) \\ N_\phi^2 &= -(u_t u^t + u_\phi u^\phi)\Delta \sin^2\theta, \\ \Delta &= r^2 + a^2 - 2Mr. \end{aligned} \tag{B2}$$

Here, a is the (dimensionful) black hole spin: $a \equiv a_* GM/c^2$. The transformation laws for vectors and one-forms are then given by

$$\begin{aligned} X^\mu &= e^\mu_{(\nu)} X^{(\nu)}, \qquad X^{(\mu)} = e^{(\mu)}_\nu X^\nu, \\ X_\mu &= e^{(\nu)}_\mu X_{(\nu)}, \qquad X_{(\mu)} = e^\nu_{(\mu)} X_\nu. \end{aligned} \tag{B3}$$

B2 Transformation of the flux

To transform the radiation flux from the BL frame (which is what the GRMHD simulations give) into the comoving frame of the fluid, we use the following method. The comoving flux is defined as

$$F_{\rm com} = \frac{\mathrm{d}E_{\rm com}}{\mathrm{d}A_{\rm com}\mathrm{d}t_{\rm com}} \equiv \frac{\mathrm{d}E_{\rm com}}{\mathrm{d}^3 V_{\rm com}}, \tag{B4}$$

where $\mathrm{d}^3 V_{\rm com}$ is the three-volume in the comoving frame. We first relate the energy in the fluid frame to that in the BL frame. Let $e_{\tilde{\Omega}}$ be the energy emitted per unit solid angle in the comoving frame. A ray of light emitted into a solid angle $\mathrm{d}\tilde{\Omega}$ in a direction $(\tilde{\theta}, \tilde{\phi})$ (where $\tilde{\theta}$ is measured with respect to the normal to the disc, i.e. the $e_{(\theta)}$ direction, and the $\tilde{\phi} = 0$ direction is arbitrary) will then have an energy-momentum four-vector given by

$$\mathrm{d}p^{(\mu)} = e_{\tilde{\Omega}} \mathrm{d}\tilde{\Omega}(1, \sin\tilde{\theta}\sin\tilde{\phi}, \cos\tilde{\theta}, \sin\tilde{\theta}\cos\tilde{\phi}), \tag{B5}$$

or, lowering the index, and remembering that the metric in the comoving frame is $\eta_{(\alpha)(\beta)} = \mathrm{diag}(-1, 1, 1, 1)$,

$$\mathrm{d}p_{(\mu)} = e_{\tilde{\Omega}} \mathrm{d}\tilde{\Omega}(-1, \sin\tilde{\theta}\sin\tilde{\phi}, \cos\tilde{\theta}, \sin\tilde{\theta}\cos\tilde{\phi}). \tag{B6}$$

Transforming this into the BL frame, we get

$$\mathrm{d}p_\mu = e^{(\nu)}_\mu \mathrm{d}p_{(\nu)}. \tag{B7}$$

The energy-at-infinity of that ray as measured in the BL frame then is

$$\mathrm{d}E = -\mathrm{d}p_t = -e^{(\nu)}_t \mathrm{d}p_{(\nu)}. \tag{B8}$$

The total energy emitted in all directions is

$$E = \int \mathrm{d}E = -e_t^{(\nu)} \int \mathrm{d}p_{(\nu)} \tag{B9}$$

$$= -e_t^{(\nu)} \int \mathrm{d}\tilde{\Omega} e_{\tilde{\Omega}} (-1, \sin\tilde{\theta}\sin\tilde{\phi}, \cos\tilde{\theta}, \sin\tilde{\theta}\cos\tilde{\phi}). \tag{B10}$$

The emission profiles we are interested in are isotropic ($e_{\tilde{\Omega}} =$ constant) or limb-darkened ($e_{\tilde{\Omega}} \propto 2 + 3\cos\tilde{\theta}$). For both of these, the second and fourth terms in the brackets vanish. The third term is multiplied by $e_t^{(\theta)} \propto u_\theta = 0$ for the thin discs that we consider here, for which the fluid velocity is purely in the equatorial plane. So we are left with

$$E = -u_t \int \mathrm{d}\tilde{\Omega} e_{\tilde{\Omega}} = -u_t E_{\mathrm{com}}. \tag{B11}$$

Next, we need to transform the three-volume $\mathrm{d}^3V_{\mathrm{com}}$. Consider first a four-volume in the BL frame bounded by $\mathrm{d}t$, $\mathrm{d}r$, $\mathrm{d}\theta$ and $\mathrm{d}\phi$. The proper four-volume $\sqrt{-g}\mathrm{d}t\mathrm{d}r\mathrm{d}\theta\mathrm{d}\phi = (\sqrt{-g_{tr\phi}}\mathrm{d}t\mathrm{d}r\mathrm{d}\phi)(\sqrt{g_{\theta\theta}}\mathrm{d}\theta)$ is an invariant. (Here, g is the determinant of the covariant BL metric, and $g_{tr\phi}$ is the determinant of the $t - r - \phi$ part of the metric.) Also, since the transformation into the comoving frame of the fluid involves a boost perpendicular to the θ-direction, the proper length in the θ-direction (which is the term in the second set of brackets in the last expression) is also invariant. [This can be checked explicitly by examining the transformation of the vector $X^\mu = (0, 0, \mathrm{d}\theta, 0)$ into the comoving frame.] Therefore, the proper three-volume $\sqrt{-g_{tr\phi}}\mathrm{d}t\mathrm{d}r\mathrm{d}\phi$ is also invariant. We therefore have

$$\begin{aligned} \mathrm{d}^3V_{\mathrm{com}} &= \sqrt{-g_{tr\phi}}\mathrm{d}t\mathrm{d}r\mathrm{d}\phi \\ &= r\mathrm{d}r\mathrm{d}\phi\mathrm{d}t \quad \text{in the equatorial plane.} \end{aligned} \tag{B12}$$

The comoving flux then becomes

$$F_{\mathrm{com}} = \frac{\mathrm{d}E}{(-u_t)r\mathrm{d}r\mathrm{d}\phi\mathrm{d}t} \tag{B13}$$

$$= \frac{F}{-u_t}, \tag{B14}$$

which is the required transformation for the flux.

APPENDIX C: RAY-TRACING GRID

The grid in the image plane is generated using plane polar coordinates (b, β). The radial grid points form a geometric series, $b_m = b_0 q^m$, $m = 0,\ldots, N_b$, where q is a number slightly larger than unity. This gives us high resolution close to the centre of the image plane, which is necessary for resolving the inner region of the accretion disc. The spacing in the angular direction is linear: $\beta_n = \beta_0 + n\delta\beta$, $n = 0,\ldots, N_\beta$. In addition, the grid is 'squeezed' along the direction defined by the projection of the black hole spin axis on to the image plane (the 'y'-axis), by an amount proportional to $\cos i$, to account for the inclination of the observer. Therefore, the radial grid becomes a set of concentric ellipses; the Cartesian coordinates of the grid vertices are $x_{mn} = b_m \cos\beta_n$, $y_{mn} = b_m \sin\beta_n \cos i$. We choose $b_0 = 1$, which is inside the black hole shadow for all spins and inclinations, i.e. it is small enough that any rays with $b < b_0$ fall into the black hole and can therefore be ignored. We also choose $b_{N_b} = 10\,000$, which is large enough to correctly produce the low-energy end of the spectrum in the energy range of interest (0.1–10 keV).

The flux in equation (2) then becomes

$$F_{\mathrm{obs}} = \frac{1}{D^2} \int I_\nu \,\mathrm{d}x\,\mathrm{d}y \tag{C1}$$

$$= \frac{\cos i}{D^2} \int I_\nu\, b\,\mathrm{d}b\,\mathrm{d}\beta \tag{C2}$$

$$= \frac{\cos i}{D^2} \int I_\nu\, b^2\,\mathrm{d}(\log b)\,\mathrm{d}\beta. \tag{C3}$$

Since the values of $\log b$ and β are equally spaced, we can now use a higher order integration method like the Simpson's one-third rule to perform the integration (see e.g. Abramowitz & Stegun 1972). This gives considerably higher accuracy and faster convergence than a naïve approach that simply sums up the product of I_ν in each grid cell with the area of that cell.

This paper has been typeset from a TEX/LATEX file prepared by the author.